Supplement of Biogeosciences, 17, 3943–3960, 2020
https://doi.org/10.5194/bg-17-3943-2020-supplement

Biogeosciences Open Access

Supplement of

Characterizing deepwater oxygen variability and seafloor community responses using a novel autonomous lander

Natalya D. Gallo et al.

Correspondence to: Natalya D. Gallo (ndgallo@ucsd.edu)

Supplement 1A

SphereCam Manual from Subaqua Imaging Systems (the manual is 10 pages long and begins on the next page)

SUBAQUA
IMAGING SYSTEMS INC
1134 Opal St, San Diego, CA 92109, USA – Ph: (858) 414 0383 – Fax (858) 4834884 – www.subaquaimaging.com

The photos that follow explain how to operate the TIMELAPSE ASSEMBLY.

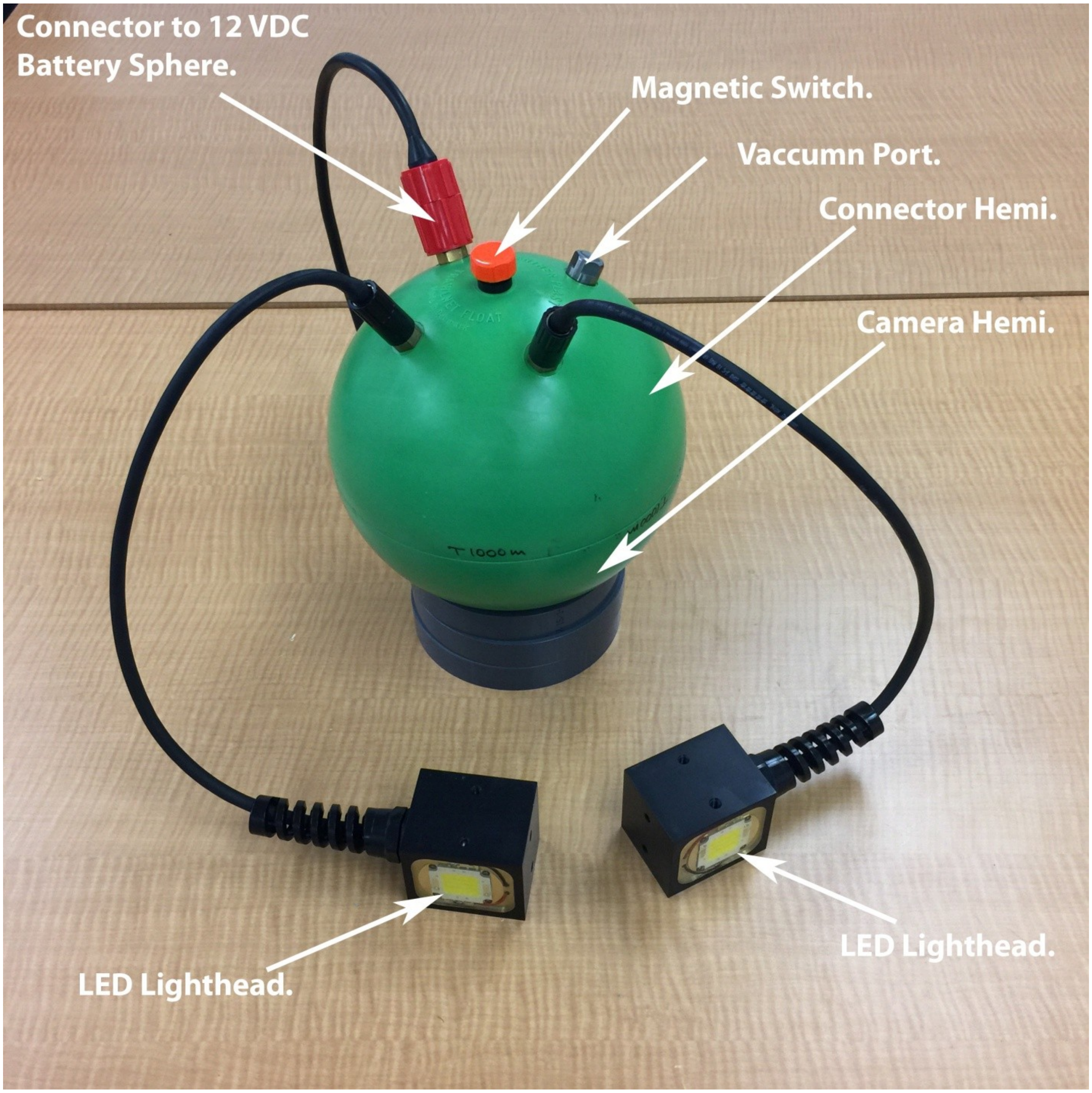

Figure 1 Overview. The camera is located in the lower hemisphere and the components for the lights are located in the upper hemisphere.

The Sphere-Cam uses our existing time-lapse assembly. We tested many small cameras before we choose the one that we use in it. The model is the Mobius Action Camera (https://www.mobius-actioncam.com/). The camera has become very popular with a range of users in particular, Radio Control airplane and drone users. There are some resources online that will help if you ever need them:

- Camera related software and owner's manual can be used when the camera is connected to a computer via the USB port. For the latest software check here: https://www.mobius-actioncam.com/downloads-info/
- To access the cameras settings download the program Msetup.zip
- There is an excellent support forum for the camera here: https://www.rcgroups.com/forums/showpost.php?p=25170910&postcount=4

The USB port and MicroSD card have been positioned within the camera sphere in such a way that you should be able to do everything needed without ever having to remove the camera.

SUBAQUA
IMAGING SYSTEMS INC
1134 Opal St, San Diego, CA 92109, USA – Ph: (858) 414 0383 – Fax (858) 4834884 – www.subaquaimaging.com

Camera Hemisphere

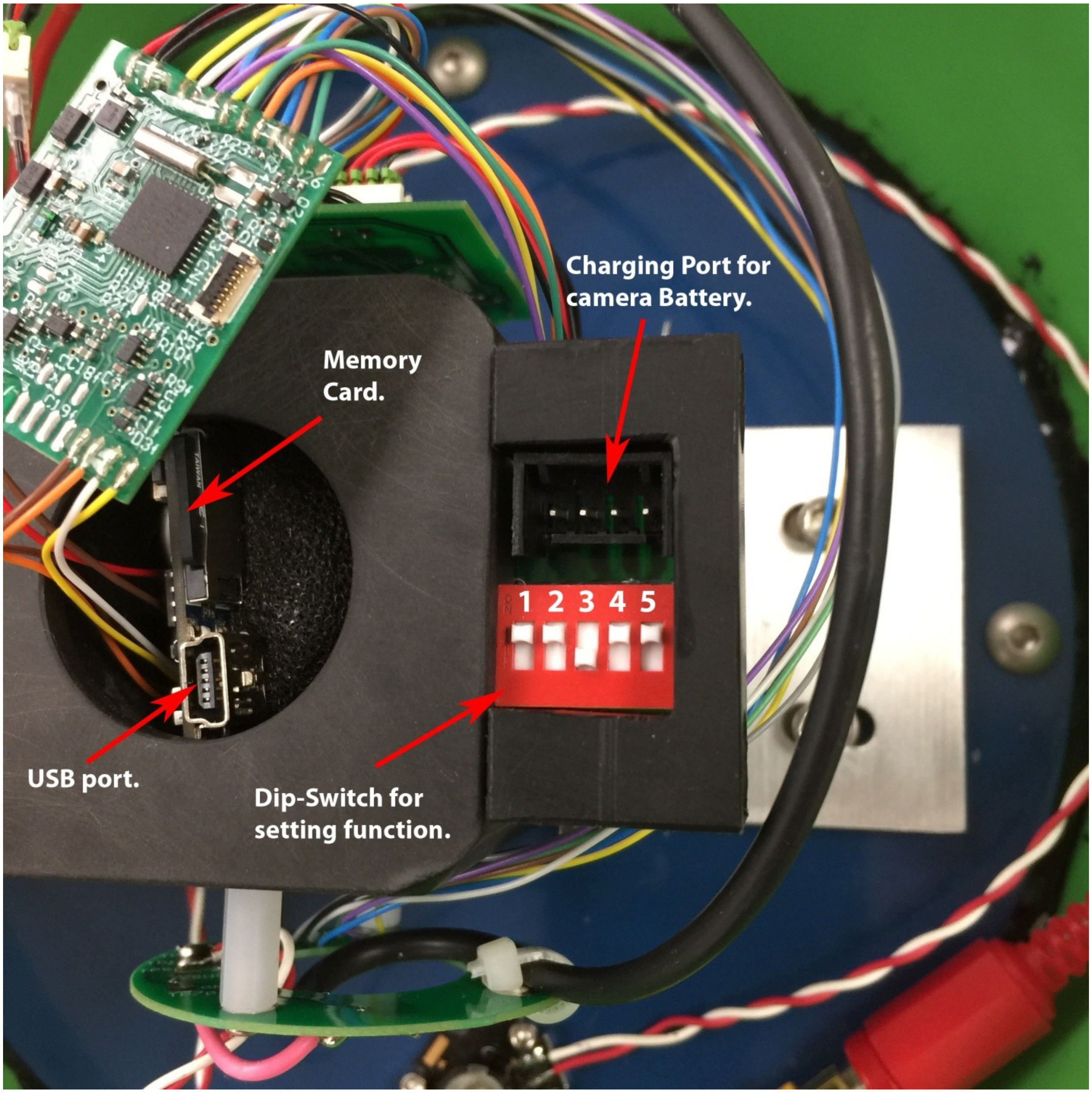

Figure 2 The Timelapse camera sphere data can be downloaded using the USB port or the Memory Card can be removed and replaced. The battery camera can be charged using the charging port next to the dip-switch. The dip-switch in the photo is in the 1101 (Every 10 min, 10 sec of Video).

1134 Opal St, San Diego, CA 92109, USA – Ph: (858) 414 0383 – Fax (858) 4834884 – www.subaquaimaging.com

1. The time lapse intervals can be set by adjusting the dip-switches. Note that power must be cycled to allow the changes in settings to be read into memory.
    a. The numbers in the table below are read from left to right corresponding with switch #1 through #4. Switch #5 is NOT USED.
    b. A "0" indicates that the switch should be in the "off" position. A "1" indicates that the switch should be in the "on" position. A switch is "on" when it is slid all the way up, next to the number on the body.
    c. **EXAMPLE:** 1000 means switch 1 on, switches 2,3 & 4 are off.

Option	DIP-SWITCH POSITIONS	Function
0	0000	Video
1	1000	30-second Photo
2	0100	1-minute Photo
3	1100	2-minute Photo
4	0010	5-minute Photo
5	1010	10-minute Photo
6	0110	15-minute Photo
7	1110	30-minute Photo
8	0001	60-minute Photo
9	1001	Every 5 Mins, 1 Mins Video
10	0101	Every 1/2 Hrs, 5 Mins Video
11	1101	Every 10 min, 10 sec of Video
12	0011	Every 20 min, 20 sec of Video
13	1011	Every 30 min, 30 sec of Video
14	0111	Every 60 min, 60sec Video
15	1111	DORMANT

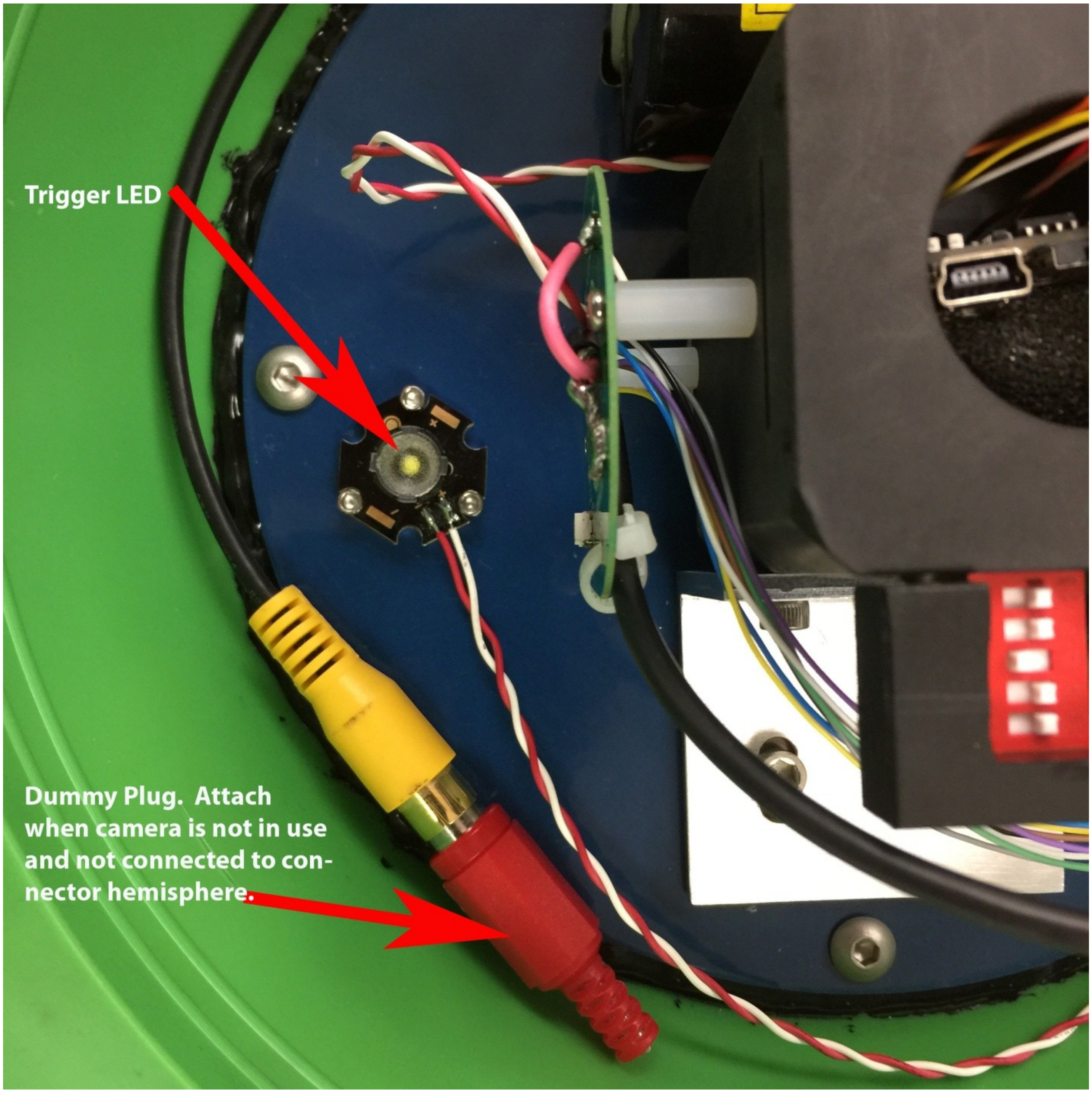

Figure 3 The camera has a small Trigger LED that activates a photo-relay in the connector hs. Do not block the LED. The magnetic release attached to the connector hs is connected to the camera via a RCA cable. Replace the dummy plug when not in use.

SUBAQUA
IMAGING SYSTEMS INC
1134 Opal St, San Diego, CA 92109, USA – Ph: (858) 414 0383 – Fax (858) 4834884 – www.subaquaimaging.com

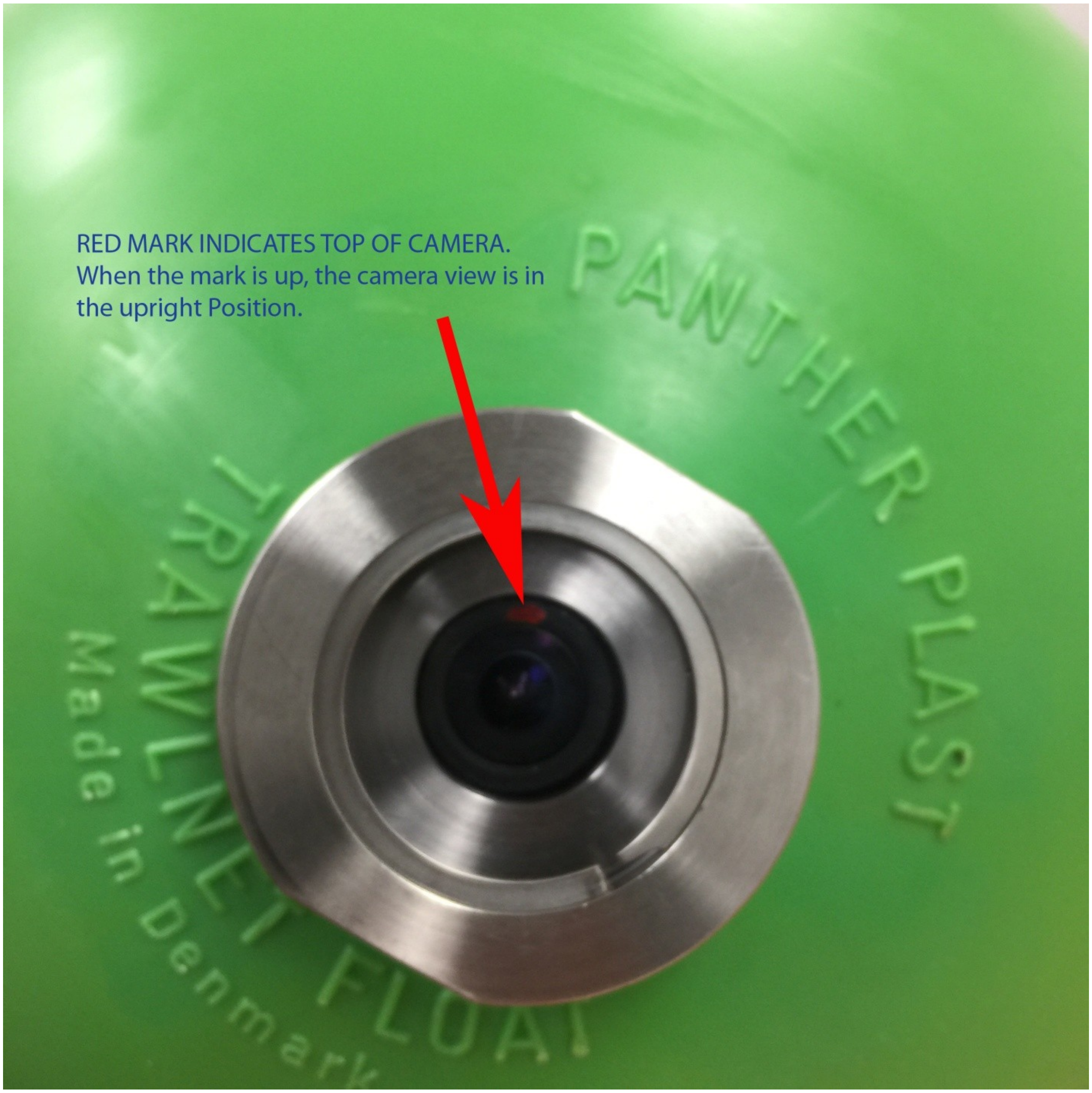

Figure 4 The window port located on the bottom of the camra hemisphere. The red mark on the lens indicates the upright positon.

Connector Hemisphere

The Connector Hemisphere has five ports:

1. 12 VDC power for lights only (the camera has it's own battery within the camera hemisphere).
2. Vacuum Port
3. Magnetic Switch (removing the brightly colored cap activates the camera).
4. LED Light cable
5. LED Light cable

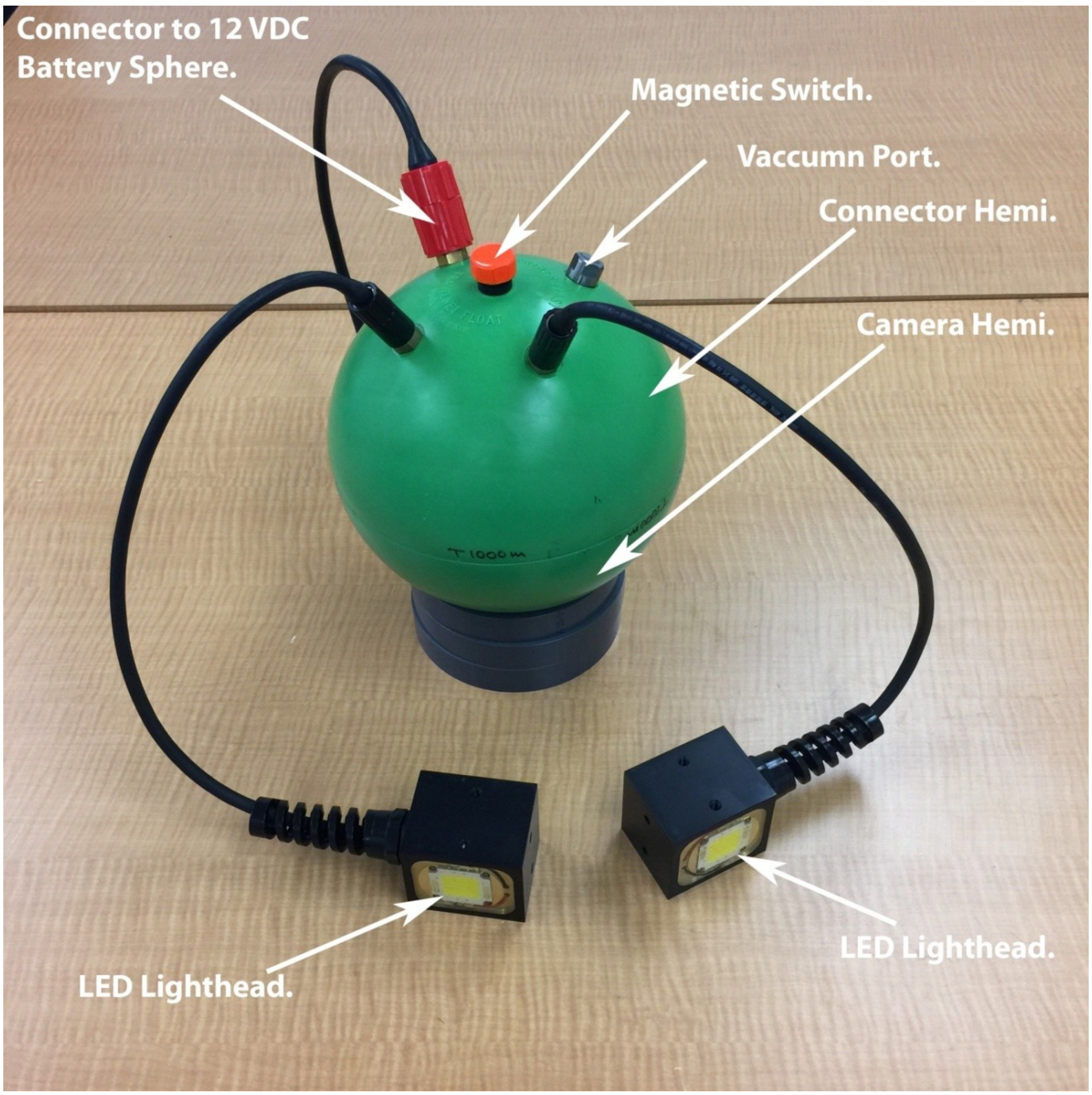

The LED drivers are the largest components in the connector sphere. There is one for each light and they are powered by the external 12 VDC power source connected to the hemisphere by the power connector. The positive leads are routed through a photo-relay which closes and allows power from the power connector to flow to them when the LED in the camera hemisphere is activated.

A 5-pin terminal strip is used to connect the output from the LED drivers to each of the LED connectors.

The positive lead of the 12VDC power runs through the 5-position terminal strip and supplies the relay and the relay switch.

A 2-postion strip located next to the photo-relay board connects the negative lead from the 12VDC connector to the LED drivers and the photo relay board.

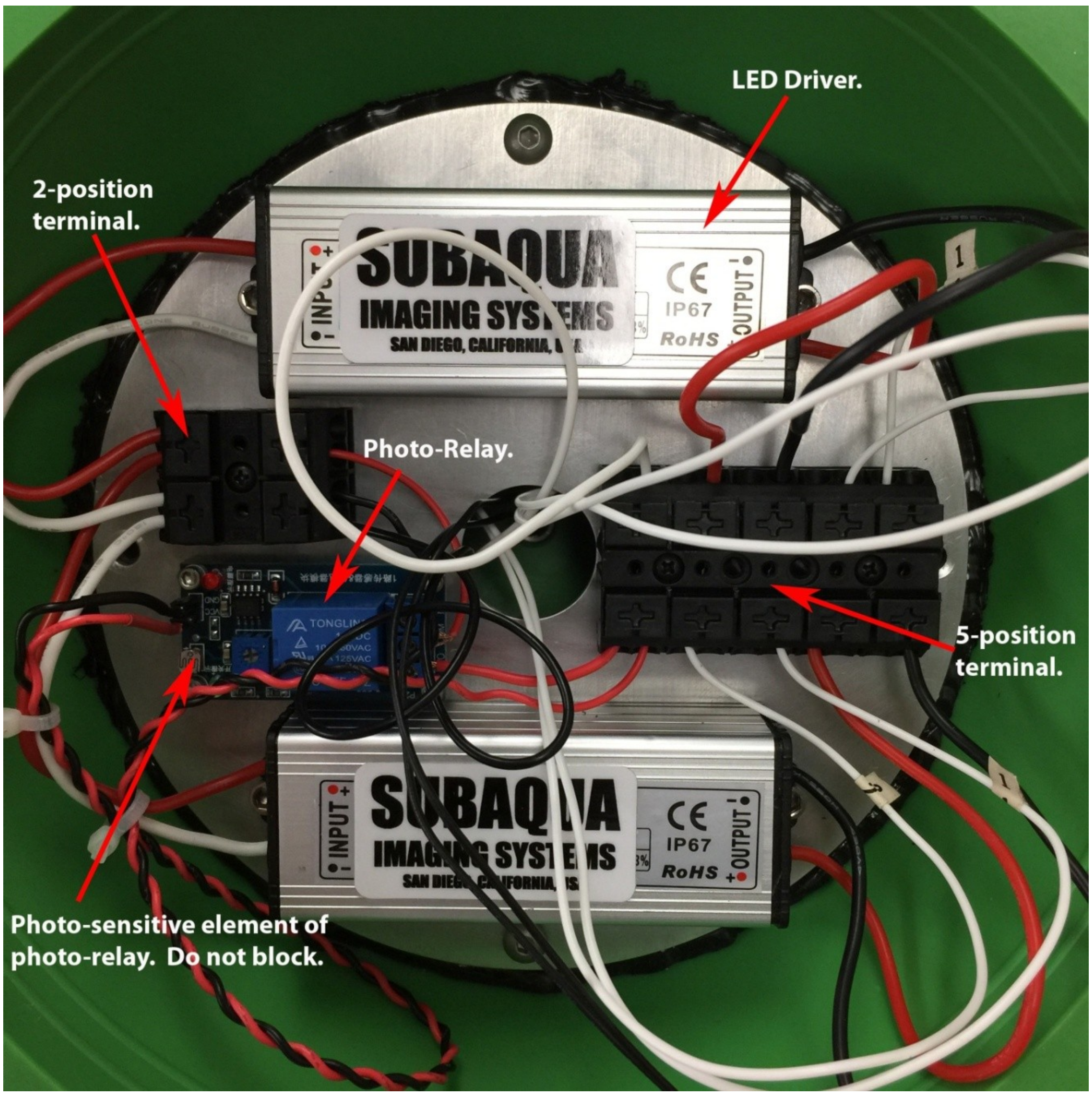

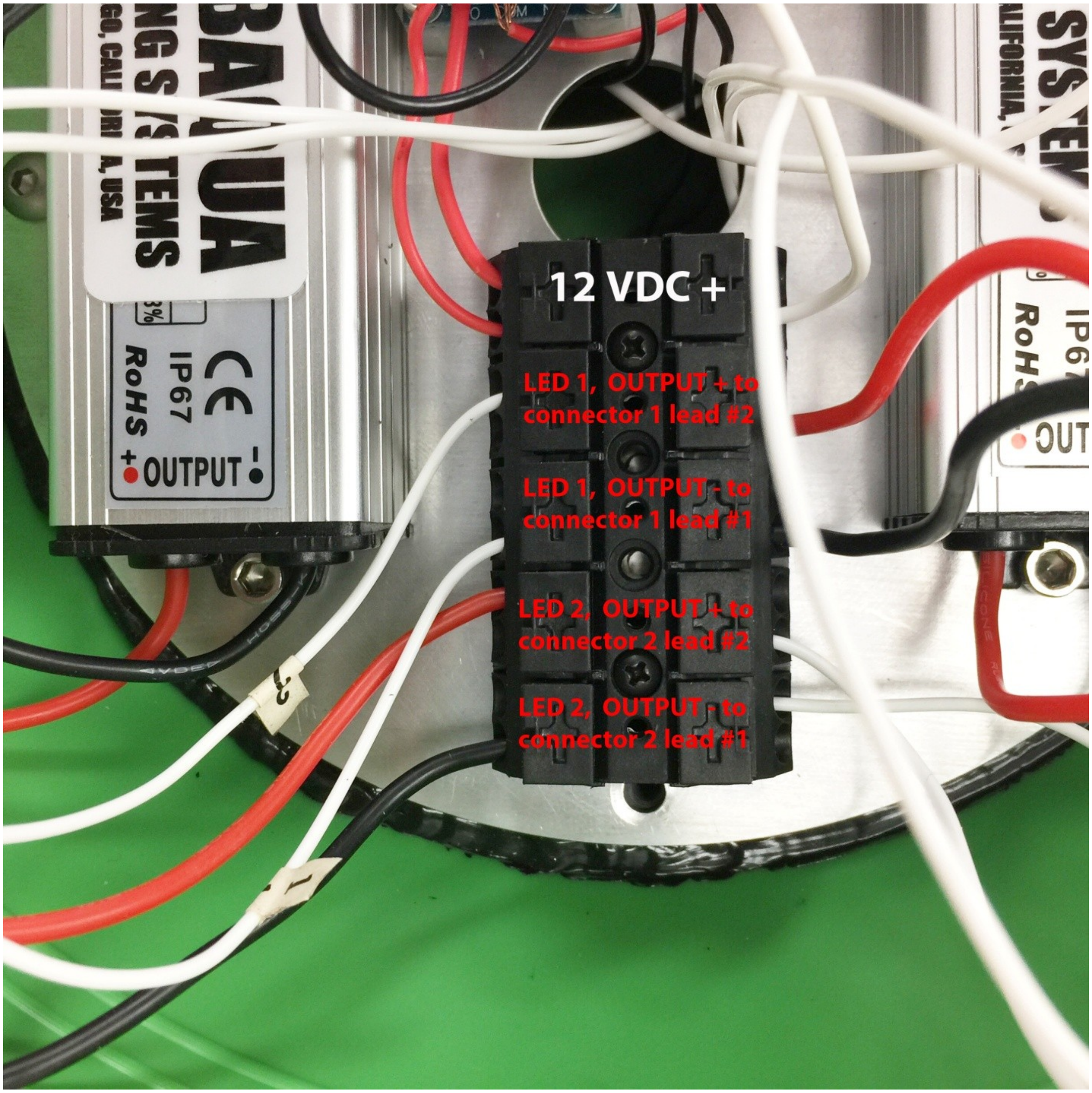

Note the RED LED above and to the right of the *"12 VDC input for relay"*. <u>This LED should be ON</u> when the external 12 VDC power is properly attached to the hemisphere, <u>regardless of whether the magnetic switch is activated or not</u>.

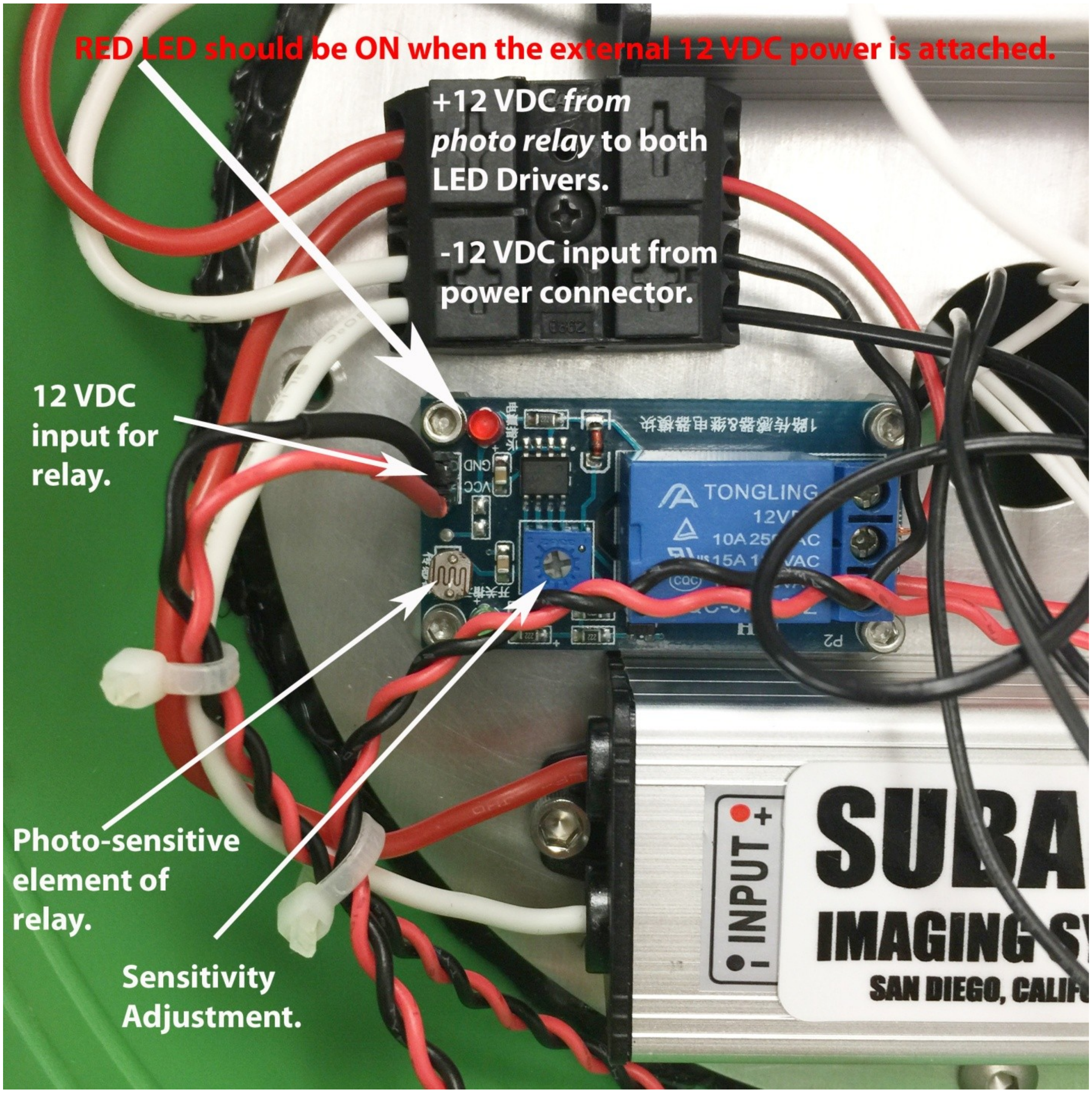

Figure 5 Note the RED LED above and to the right of the *"12 VDC input for relay"*. <u>This LED should be ON</u> when the external 12 VDC power is properly attached to the hemisphere, <u>regardless of whether the magnetic switch is activated or not</u>.

Supplement 1B

Table showing the mean and range of oxygen conditions for each deployment in oxygen saturation (%) and in oxygen partial pressure (kPa).

	D200-LJ-1	D200-LJ-2	D100-DM-Fall	D200-DM	D300-DM	D400-DM	D100-DM-Spr
Mean O_2 Sat (%)	25.60	27.97	48.67	29.35	17.25	9.91	37.36
O_2 Sat Range (%)	17.55-37.79	17.66-39.37	40.11-58.50	22.52-37.27	13.81-20.89	7.18-13.26	32.54-44.55
pO_2 (kPa)	5.50	6.01	10.33	6.32	3.77	2.20	7.94
pO_2 Range (kPa)	3.77-8.11	3.79-8.45	8.52-12.41	4.85-8.02	3.02-4.56	1.59-2.94	6.92-9.47

Supplement 1C

Table of fish species observations including deployment label, minimum and maximum depths, minimum and maximum temperature and oxygen conditions, and number of video clips each species was observed during.

Fish Species	Deployment	Depth Range (m)	Temperature (°C)	Oxygen (µmol/kg)	Number of Video Clips Observed in
Anarrhichthys ocellatus	D100-DM-Fall	99	11.25	134.40	1
Apristurus brunneus	D400-DM	399	7.27- 7.50	26.70 - 30.76	4
Cephaloscyllium ventriosum	D200-LJ-2	178	9.78 - 10.01	73.38 - 89.47	4
Chilara taylori	D200-LJ-2, D100-DM-Fall, D100-DM-Spr	98 - 178	9.42 - 11.56	49.51 - 142.43	358
Eptatretus stoutii	D200-LJ-2, D100-DM-Fall, D200-DM, D400-DM, D100-DM-Spr	98 - 399	7.10 - 11.46	22.54 - 138.67	124
Faciolella equatorialis	D200-LJ-2, D400-DM	399 - 178	7.07 - 10.00	21.55 - 90.32	130
Genyonemus lineatus	D200-LJ-2	178	9.60 - 10.12	62.04 - 91.47	11
Hydrolagus colliei	D200-LJ-2, D100-DM-Fall, D200-DM, D400-DM, D100-DM-Spr	98 - 399	7.26 - 11.46	24.76 - 138.67	79
Lycodes sp.	D200-LJ-2, D100-DM-Fall, D200-DM, D100-DM-Spr	98 - 192	9.19 - 11.60	50.18 - 144.76	283
Lyconema barbatum	D200-LJ-2, D100-DM-Spr	98 - 178	9.86 - 10.09	74.44 - 109.69	4
Lyopsetta exilis	D400-DM	399	7.18	23.02	1
Merluccius productus	D200-DM, D300-DM, D400-DM, D100-DM-Spr	98 - 399	7.47 - 9.86	29.90 - 108.68	11
Microstomus pacificus	D200-LJ-2, D400-DM	178 - 399	7.10 - 10.15	22.54 - 96.72	100
Nezumia liolepis	D400-DM	399	7.19 - 7.39	23.43 - 29.63	9
Ophiodon elongatus	D100-DM-Fall, D100-DM-Spr	98 - 99	9.63 - 11.29	103.2 - 134.3	9
Osteichthyes unknown	D200-LJ-2, D100-DM-Fall, D200-DM, D100-DM-Spr	98 - 192	9.19 - 11.89	49.51 - 146.99	414
Oxylebius pictus	D100-DM-Fall	99	11.26	136.90	1
Pacific sanddab	D200-LJ-2, D200-DM	178 - 192	9.25 - 9.79	64.30 - 91.22	21
Physiculus rastrelliger	D200-LJ-2, D100-DM-Fall, D100-DM-Spr	98 - 178	9.59 - 11.27	65.33 - 133.62	12
Raja rhina	D400-DM	399	7.15 - 7.44	23.57 - 30.20	2
Rathbunella hypoplecta	D200-LJ-2, D100-DM-Fall, D100-DM-Spr	98 - 178	9.50 - 11.89	62.04 - 146.99	318
Scorpaena gutatta	D100-DM-Fall	99	11.03	132.26	1
Sebastes caurinus	D100-DM-Fall	99	10.48 - 11.20	119.2 - 133.10	3
Sebastes diploproa	D400-DM	399	7.32	27.11	1
Sebastes elongatus	D100-DM-Fall, D100-DM-Spr	98 - 99	9.56 - 11.59	100.27 - 142.16	40
Sebastes lentiginosus	D100-DM-Fall	99	10.80 - 11.60	126.60 - 144.80	13
Sebastes miniatus	D100-DM-Fall	99	10.63 - 11.24	124.0 - 137.3	15
Sebastes ovalis	D100-DM-Fall	99	11.17 - 11.50	131.1 - 139.8	3
Sebastes paucispinis	D100-DM-Fall, D100-DM-Spr	98 -99	9.92 - 11.24	109.60 - 137.20	27
Sebastes pinniger	D100-DM-Fall, D100-DM-Spr	98 -99	9.52 - 11.89	99.15 - 146.99	78
Sebastes rosaceus	D100-DM-Fall, D100-DM-Spr	98 -99	9.64 - 11.55	106.65 - 141.20	38
Sebastes rubrivinctus	D100-DM-Fall, D100-DM-Spr	98 -99	9.66 - 11.46	104.3 - 138.7	60
Sebastes semicinctus	D200-LJ-2, D100-DM-Fall, D100-DM-Spr	98 - 178	9.42 - 11.89	74.42 - 146.99	1227
Sebastes Sp Dark orange	D100-DM-Spr	98	9.69 - 10.21	106.3 - 122.7	2
Sebastes sp Unidentified	D200-LJ-2, D100-DM-Fall, D200-DM, D100-DM-Spr	98 -192	9.03 - 11.79	58.69 - 146.22	626
Sebastolobus alascanus	D400-DM	399	7.19 - 7.49	23.41 - 30.61	38
Seriphus politus	D100-DM-Fall	99	10.92	128.90	1
Skate	D200-LJ-2	178	9.86	76.89	1
Squalus suckleyi	D200-DM	192	9.41	71.73	1
Symphurus sp	D200-LJ-2	178	9.76 - 10.29	68.87 - 97.94	15
Synodus lucioceps	D200-LJ-2, D100-DM-Fall, D200-DM	99 - 192	9.22 - 11.50	56.80 - 139.78	210
Unidentified shark	D100-DM-Fall, D200-DM	99 - 192	9.57 - 10.71	71.49 - 124.82	2
Xeneretmus latifrons	D200-LJ-2, D200-DM, D400-DM	178 - 399	7.08 - 10.28	22.27 - 95.11	324
Zalembius roseaceus	D100-DM-Fall, D100-DM-Spr	98 - 99	9.90 - 11.34	109.5 - 140.2	13
Zaniolepis frenata	D100-DM-Fall	99	10.80 - 11.31	126.6 - 137.3	5
Zaniolepis spp	D200-LJ-2, D100-DM-Fall, D200-DM, D100-DM-Spr	98 - 192	9.12 - 11.73	64.86 - 146.99	220

Supplement 1D

Periodograms are shown for each of the seven deployments. Periodograms are organized by deployment and deployment depth from shallowest (top) to deepest (bottom), and deployment depths are indicated. The dominant period identified is indicated, which corresponds to the highest peak on the periodogram. Note the differences in y-axis scale, across the periodograms: shallower deployments have a larger amplitude signal than deeper deployments. From upper left to lower right: D5 = D100-DM-Fall, D10 = D100-DM-Spr, D3 = D200-LJ-1, D4 = D200-LJ-2, D6 = D200-DM, D7 = D300-DM, D8 = D400-DM.

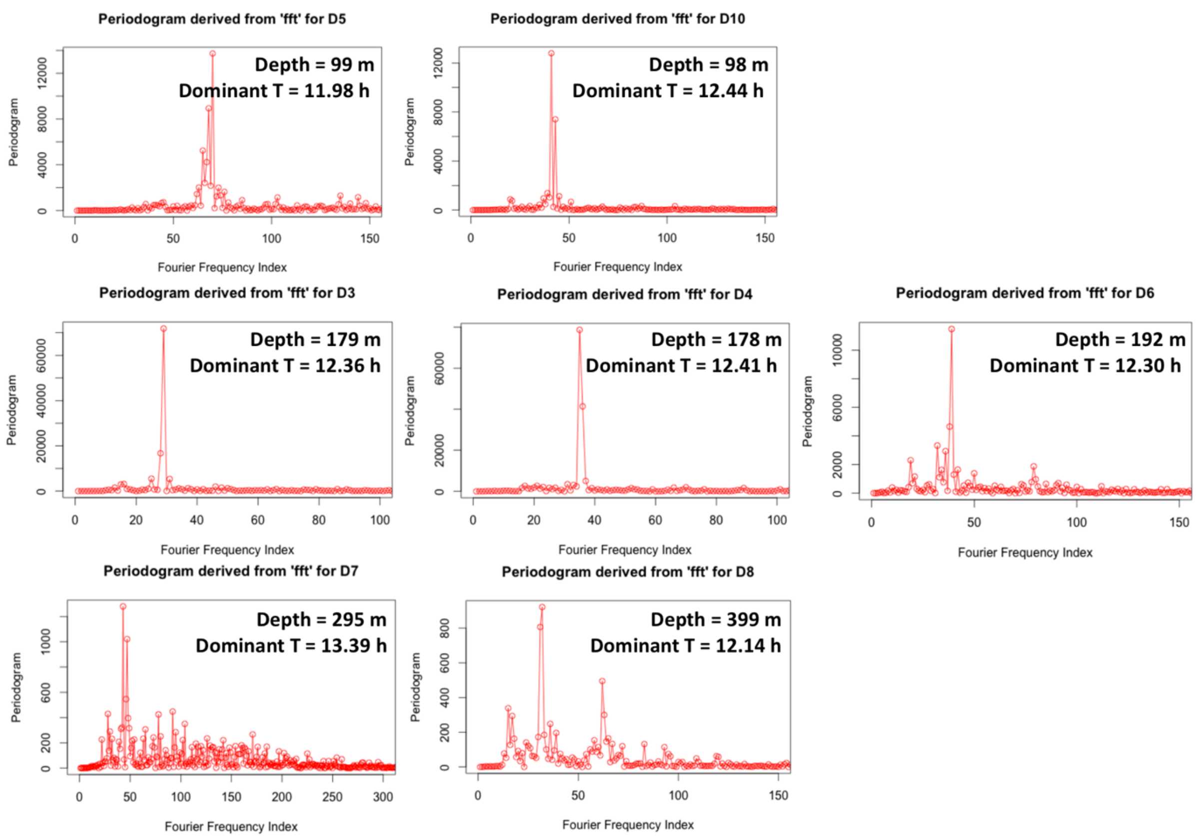

Supplement 1E

Figures showing oxygen time series for all seven deployments, as well as each time series decomposed into the deconstructed trend, daily variability, and random variance.

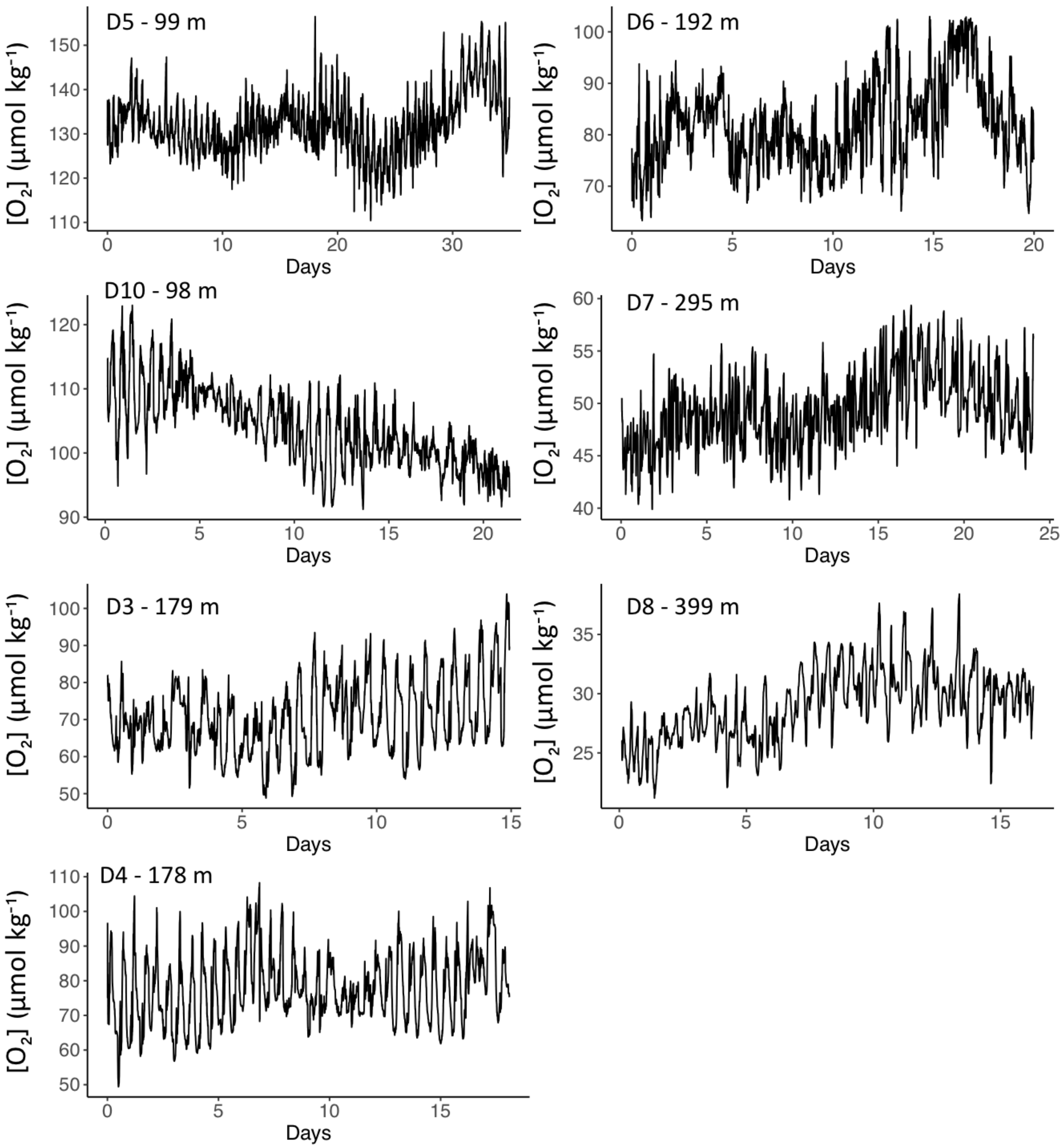

Time series of dissolved oxygen concentration with deployment time (in days) for all seven deployments. D5 = D100-DM-Fall, D10 = D100-DM-Spr, D3 = D200-LJ-1, D4 = D200-LJ-2, D6 = D200-DM, D7 = D300-DM, D8 = D400-DM.

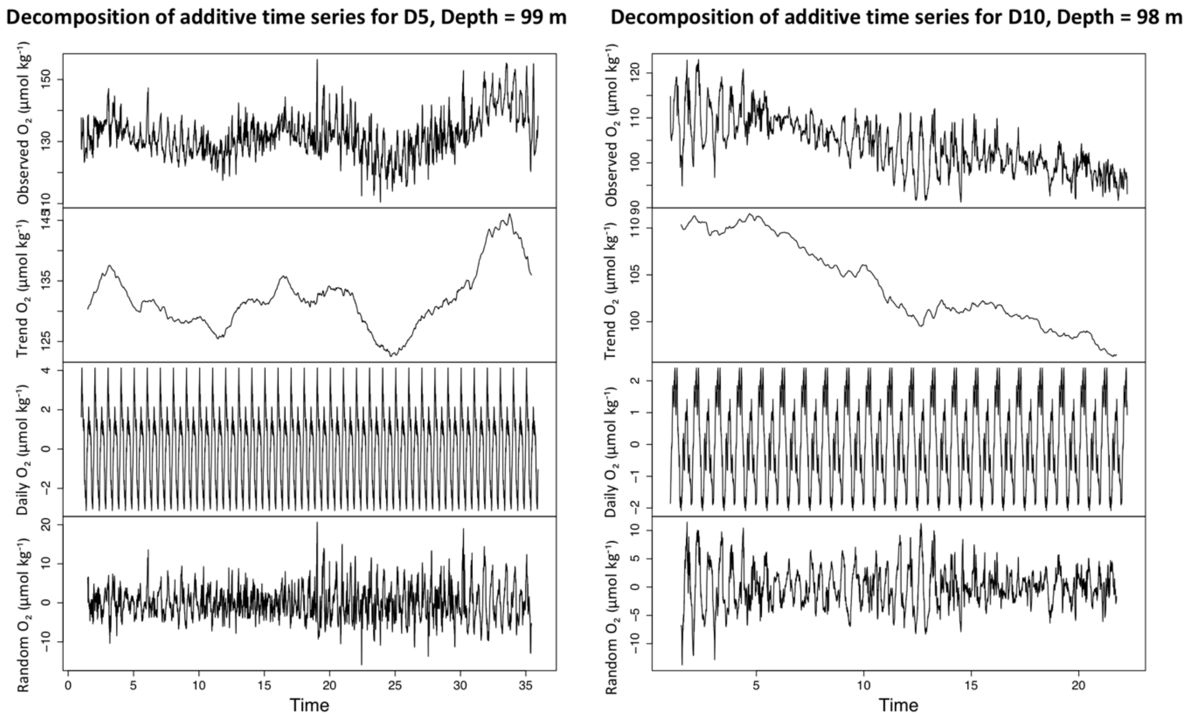

Decomposed time series of dissolved oxygen concentration for the two shallowest deployments at ~100 m on Del Mar Steeples Reef (D5 = D100-DM-Fall and D10 = D100-DM-Spr) showing the actual observations, followed by the deconstructed trend, daily variability, and random variance. Dates for deployments were: September 29-November 3, 2017 (D5) and March 8-March 29, 2018 (D10).

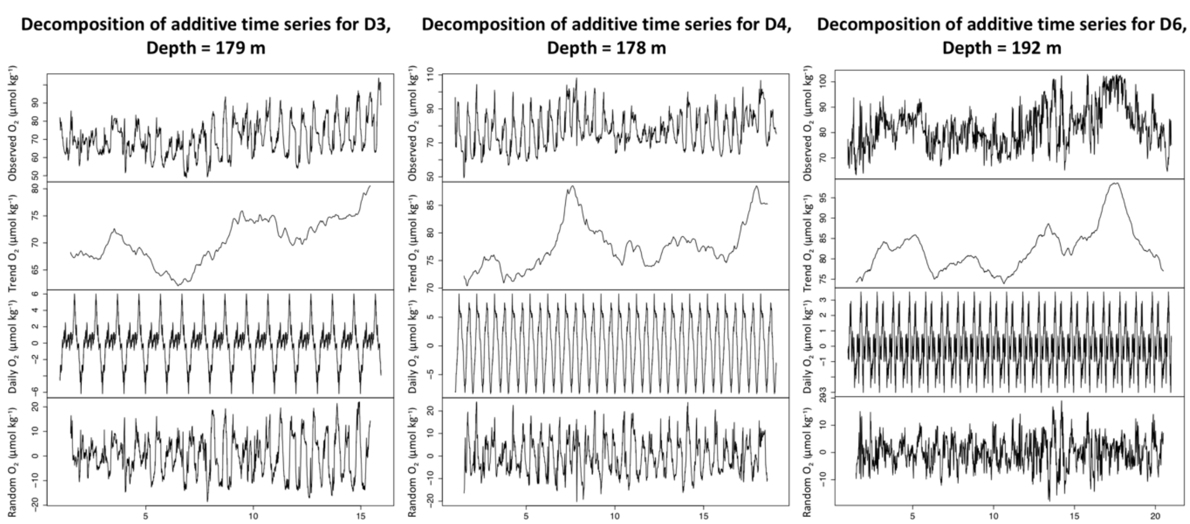

Decomposed time series of dissolved oxygen concentration for the three deployments at ~200 m (D3 = D200-LJ-1, D4 = D200-LJ-2, and D6 = D200-DM) showing the actual observations, followed by the deconstructed trend, daily variability, and random variance. Dates for deployments were: August 17-September 1, 2017 (D3), September 7-September 25, 2017 (D4), and November 9-November 29, 2017 (D6).

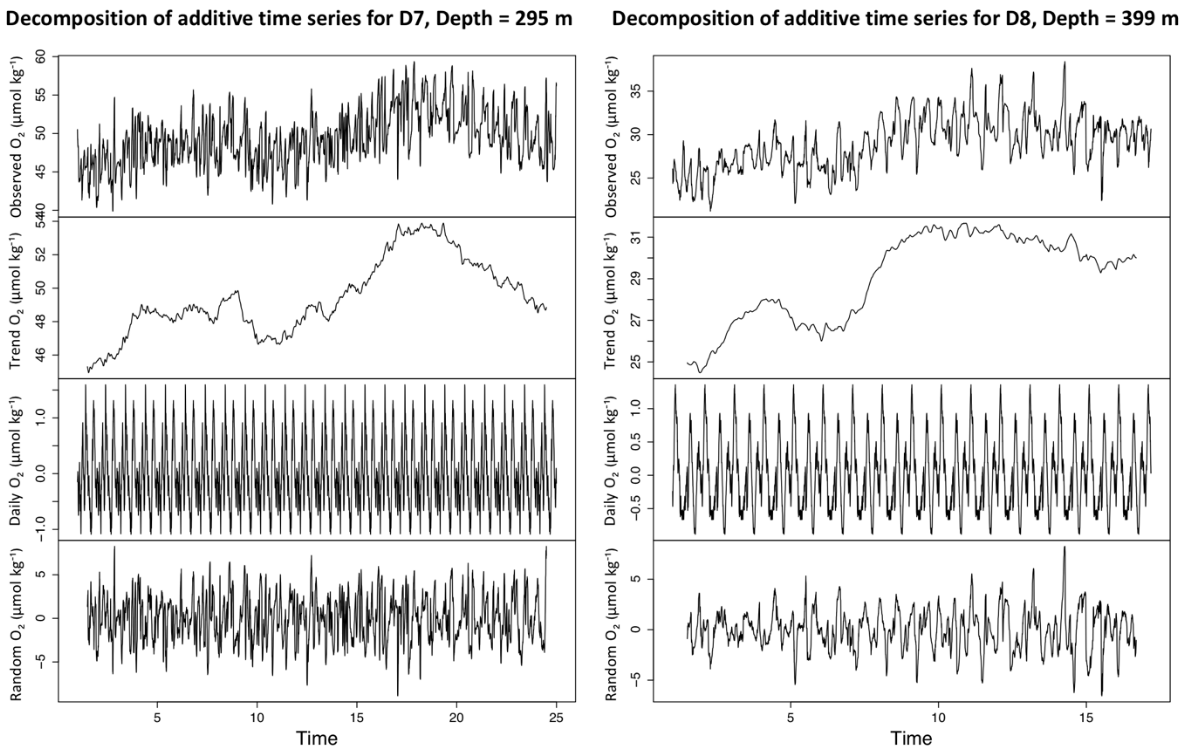

Decomposed time series of dissolved oxygen concentration for the two deepest deployments (D7 = D300-DM and D8 = D400-DM), showing the actual observations, followed by the deconstructed trend, daily variability, and random variance. Dates for deployments were: December 12, 2017-January 5, 2018 (D7) and January 23-February 8, 2018 (D8).

Supplement 1F

Figures showing relationship between tidal cycle and oxygen time series, showcasing periods from each deployment. The general pattern that emerges is that oxygen conditions tend to increase during ebb tide as the tide retreats, and decrease during flood tide as the tide rises. This is the case during all deployments, except during D300-DM.

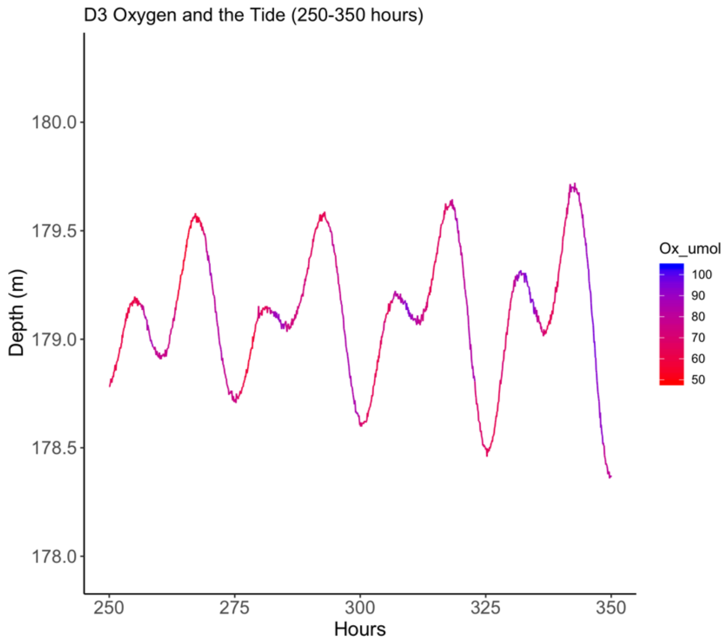

Relationship between tidal activity (viewed as changes in depth) and dissolved oxygen concentration at D3 = D200-LJ-1.

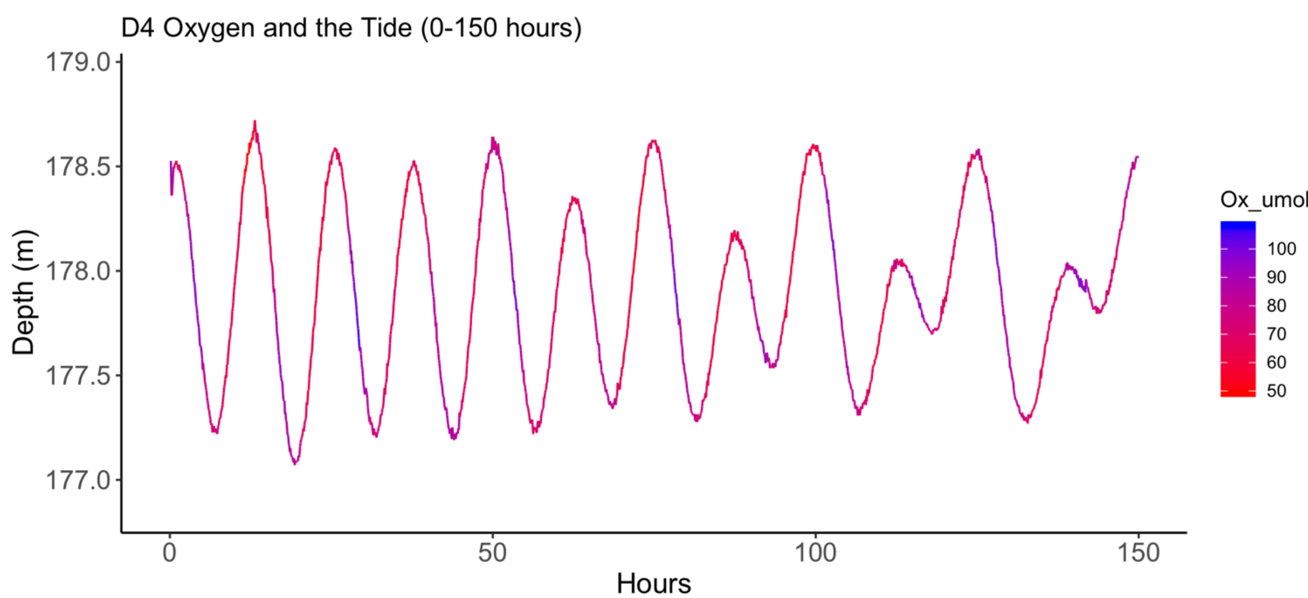

Relationship between tidal activity (viewed as changes in depth) and dissolved oxygen concentration at D4 = D200-LJ-2.

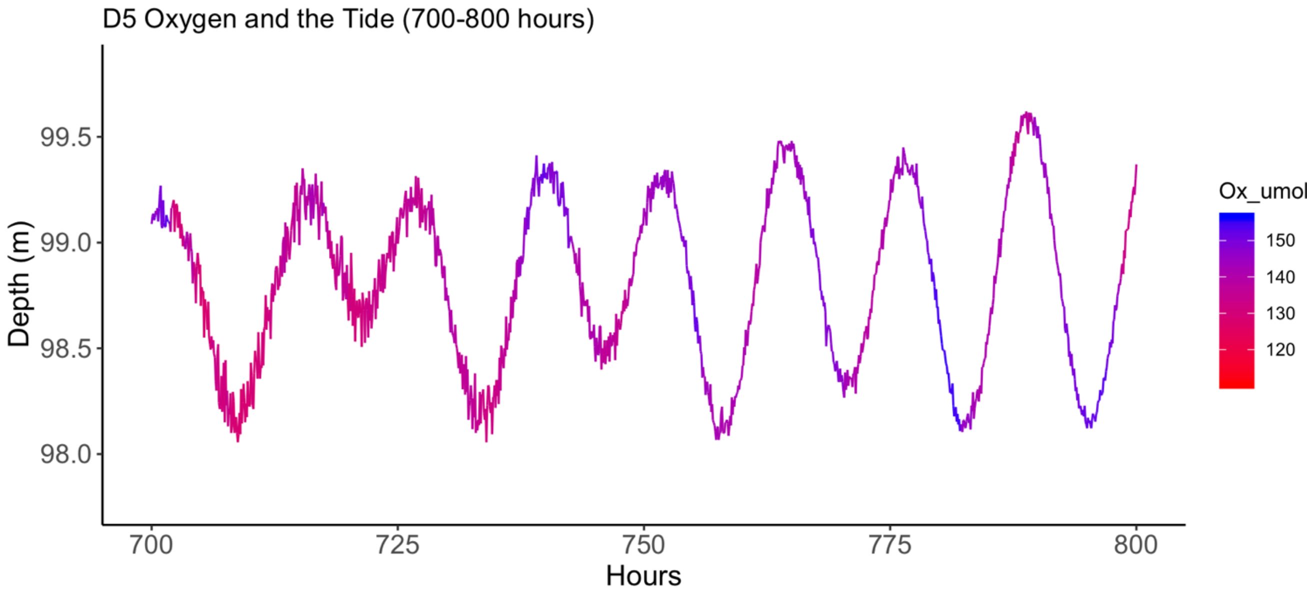

Relationship between tidal activity (viewed as changes in depth) and dissolved oxygen concentration at D5 = D100-DM-Fall.

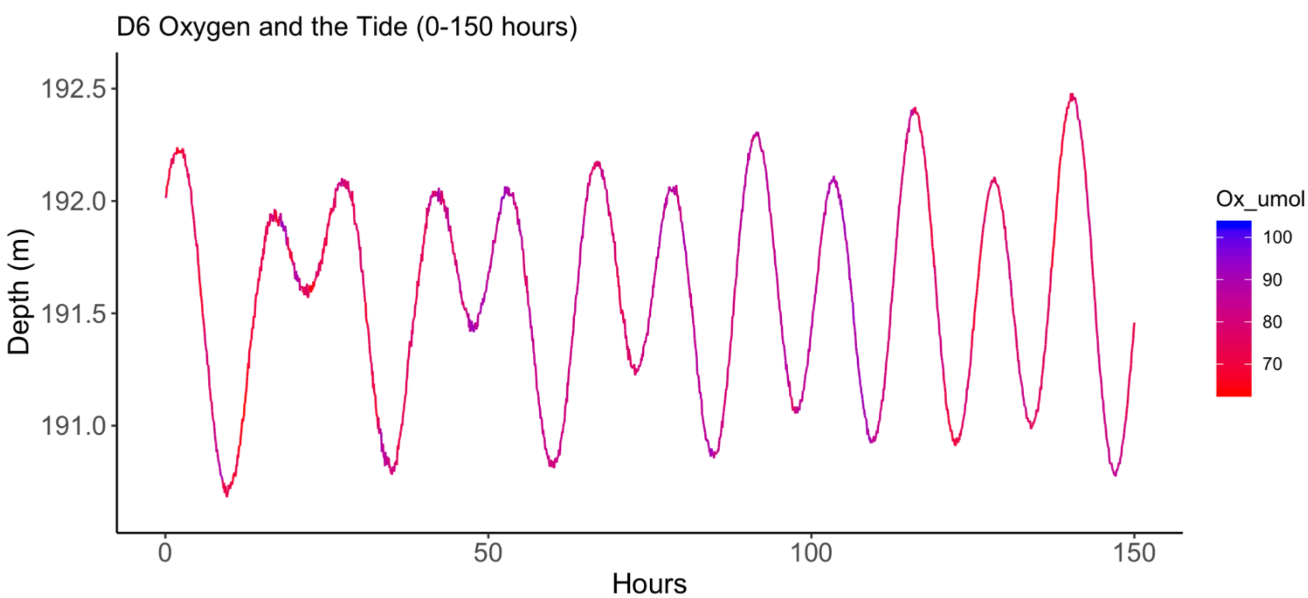

Relationship between tidal activity (viewed as changes in depth) and dissolved oxygen concentration at D6 = D200-DM.

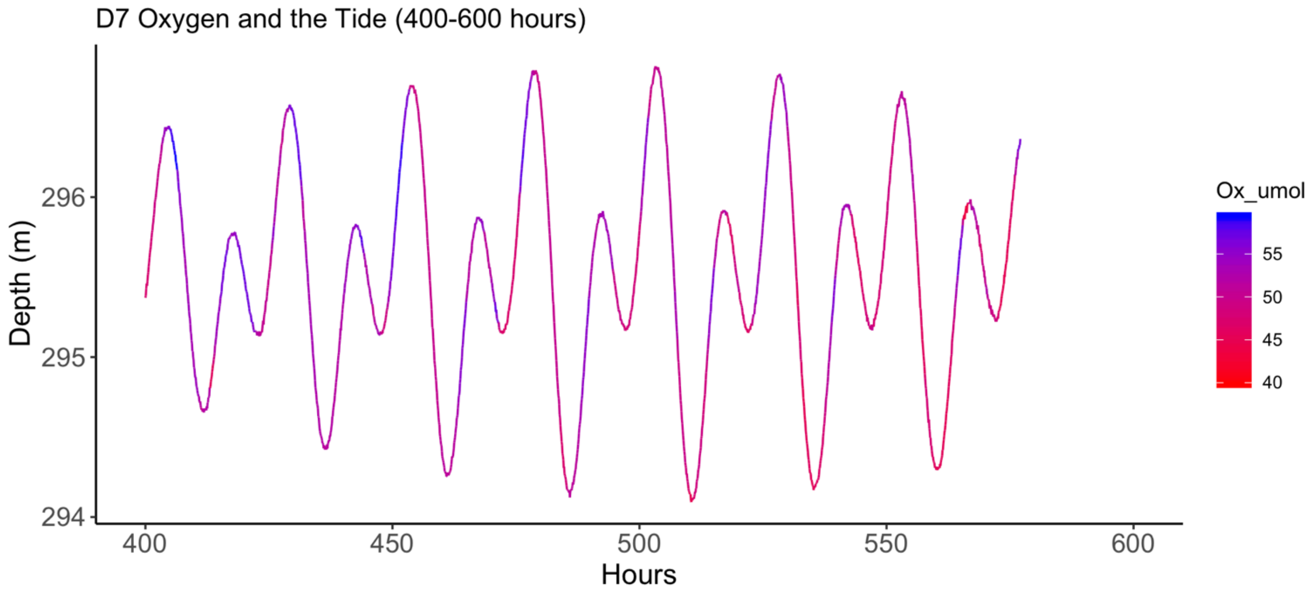

Relationship between tidal activity (viewed as changes in depth) and dissolved oxygen concentration at D7 = D300-DM. Note that at this site, oxygen increases as the tide rises, and decreases as the tide falls (in contrast to the pattern observed at all other sites).

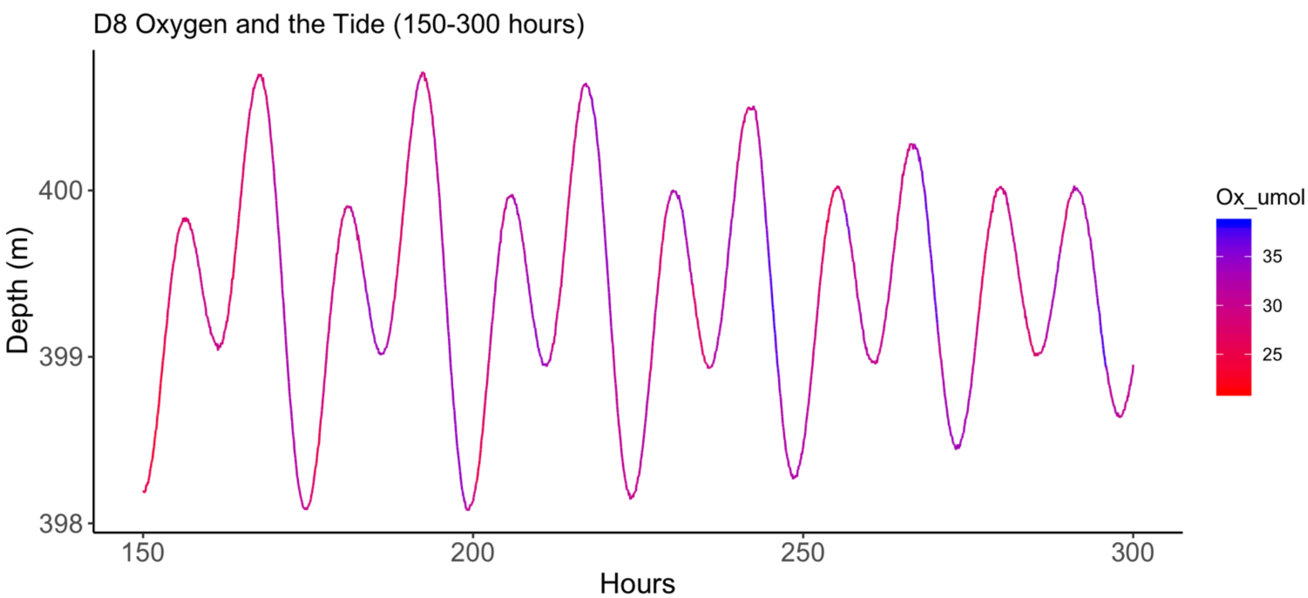

Relationship between tidal activity (viewed as changes in depth) and dissolved oxygen concentration at D8 = D400-DM.

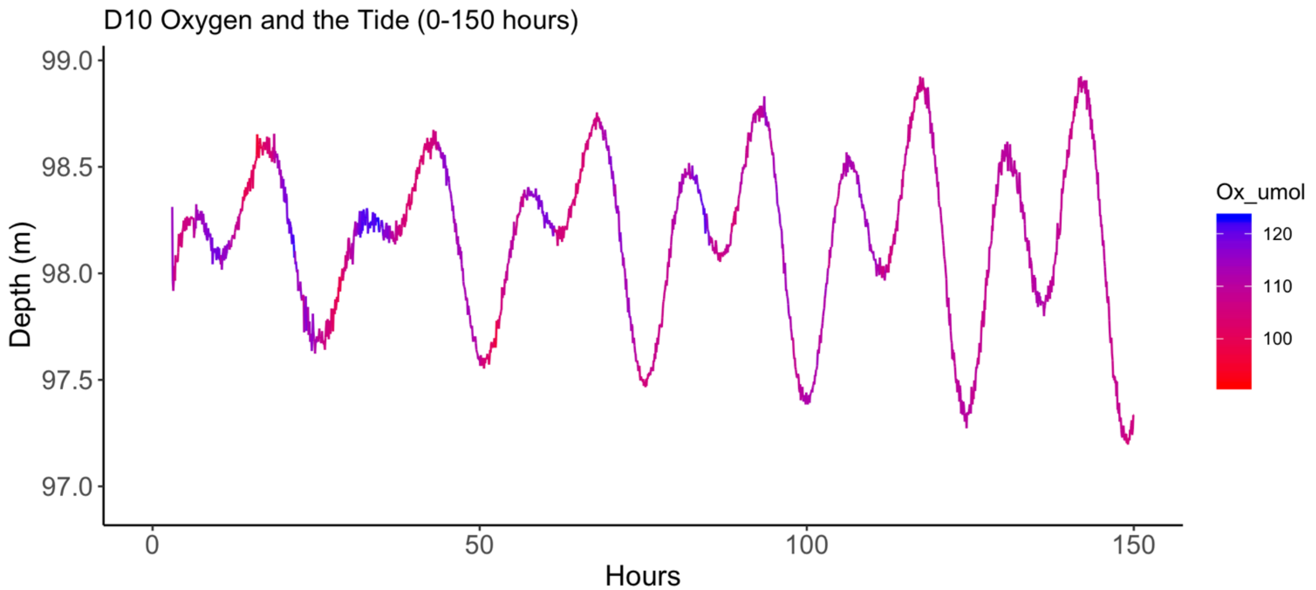

Relationship between tidal activity (viewed as changes in depth) and dissolved oxygen concentration at D10 = D100-DM-Spr.

Additionally, we examined the relationship between tidal patterns and oxygen variability to see if larger tidal variability during spring tides resulted in greater oxygen variability. When plotting oxygen and depth time series, no obvious patterns are apparent.

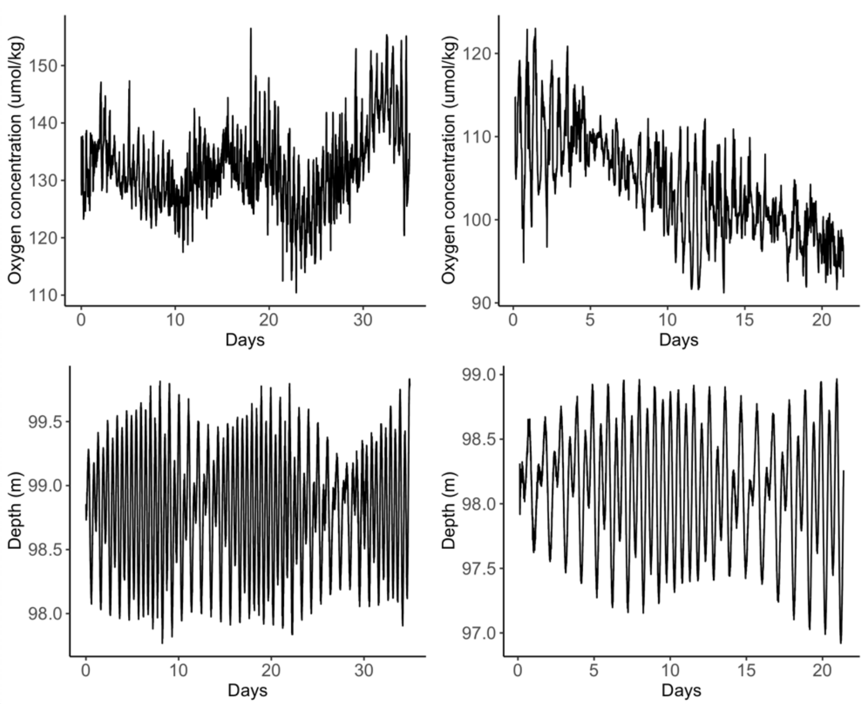

Oxygen (top) and depth (bottom) time series for the two 100 m deployments: D100-DM-Fall is on the left and D100-DM-Spr is on the right. For D100-DM-Spr, periods of higher oxygen variability visible in the time series appear to occur during periods of time when the tidal signal is weaker, as opposed to the contrary.

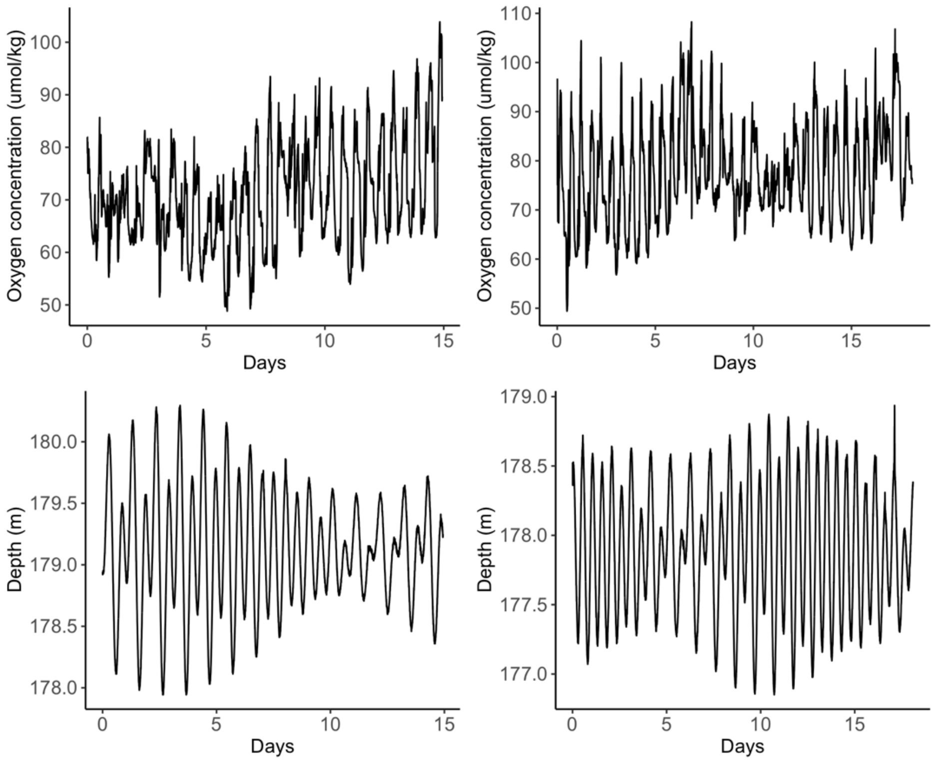

Oxygen (top) and depth (bottom) time series for the two ~200 m deployments near the Scripps Reserve: D200-LJ-1 is on the left and D200-LJ-2 is on the right.

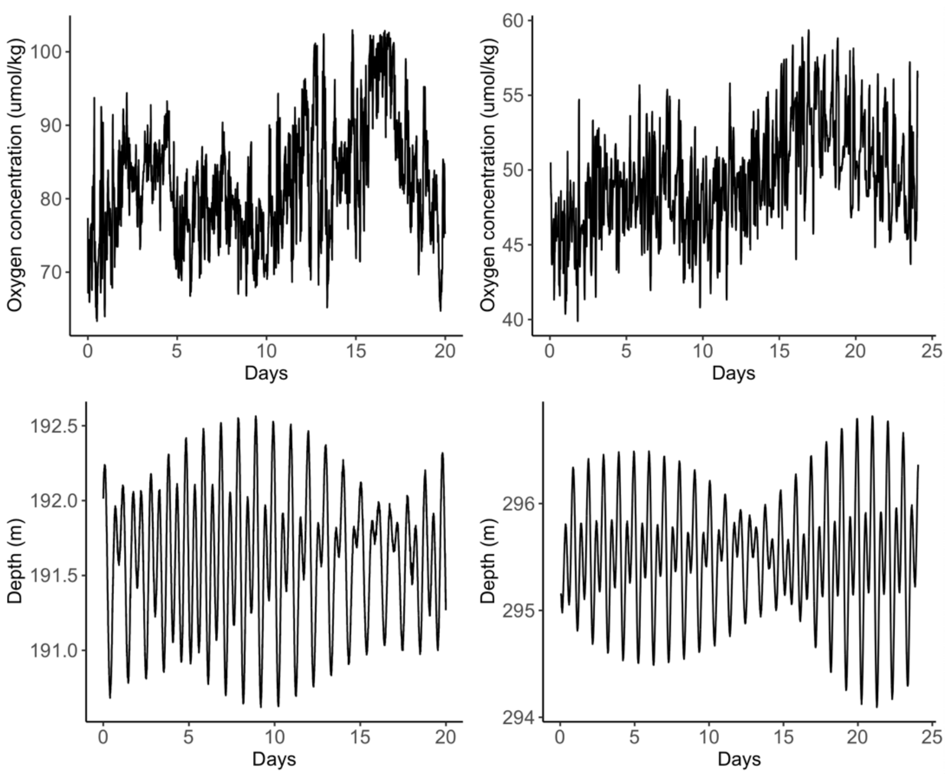

Oxygen (top) and depth (bottom) time series for the D200-DM deployment on the left and the D300-DM deployment on the right. No clear patterns can be seen between tidal patterns and oxygen variability.

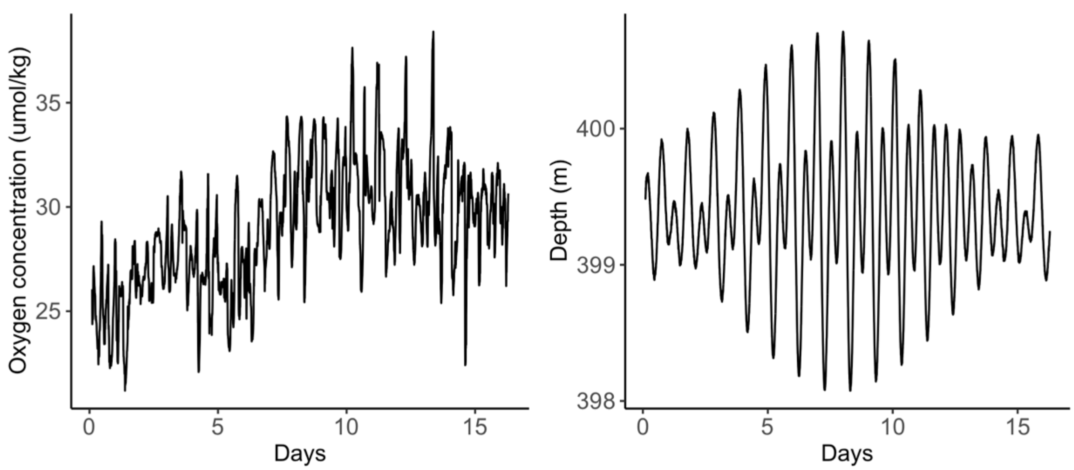

Oxygen (left) and depth (right) time series for the D400-DM deployment. No clear patterns can be seen between tidal patterns and oxygen variability.

Additionally, we examined the relationship between tidal strength and oxygen variability by determining the range in oxygen concentration and the range in depth observed during each day of each deployment. We then examined if there was a linear relationship between tidal range and oxygen concentration range. We hypothesized that oxygen variability would increase during stronger tidal periods (i.e. when the range in depth during a one day period was higher). However, no positive relationships were observed. In the case of D100-DM-Spr, D200-LJ-1, and D200-LJ-2, the reverse appears to be true. Periods with higher daily oxygen variability (i.e. a larger daily range in oxygen concentration) were correlated with a smaller daily range in depth, indicating a weaker tidal cycle.

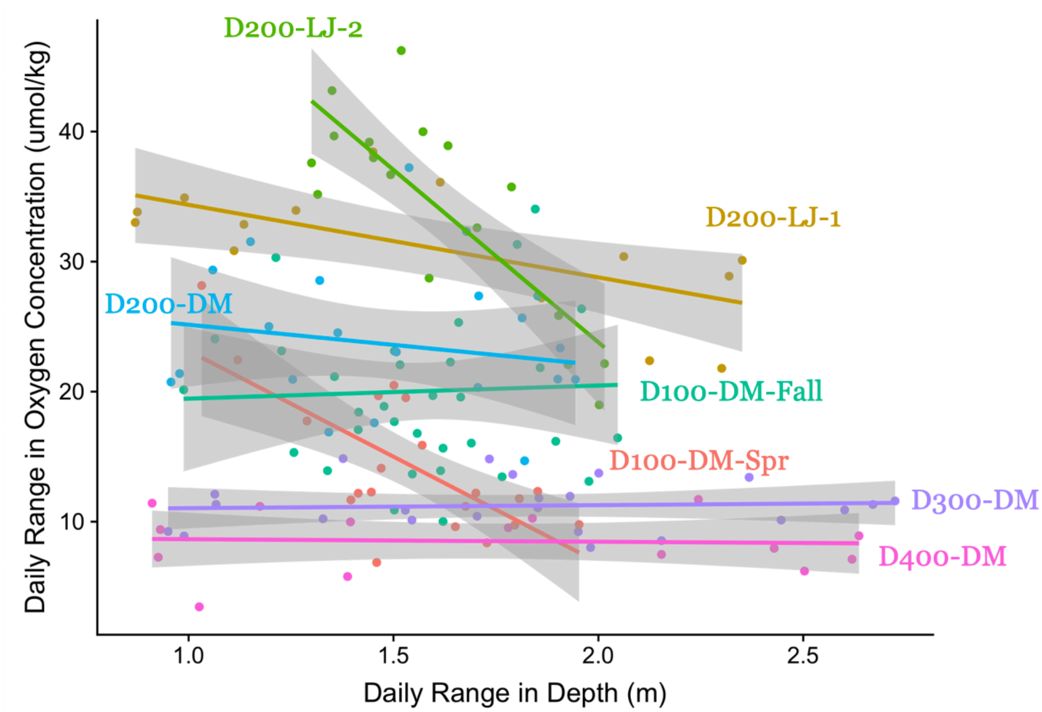

Relationship between daily tidal strength and daily range in oxygen concentration for each deployment. Points represent individual days of the deployment time series.

Supplement 1G

To look at patterns in cross-sectional structures of water temperature and dissolved oxygen across the shelf and slope, and to look at how these spatial patterns change seasonally, we extracted data from CalCOFI stations 93.3 28, 93.3 30, 93.3 35, and 93.3 40 and examined the CTD profiles for these stations during the deployment period (August 2017-March 2018).

Four cruises were relevant to examine, however, cruise 1802SH was shortened due to the government shutdown and therefore only one of the four stations (93.3 30) was sampled. As such, we focused this additional analysis on just the three cruises (1708SR – August 2017, 1711SR – November 2017, and 1804SH – April 2018). Temperature and oxygen profiles for these four stations across the three relevant cruises are shown.

From these profiles, we see that in the spring (April 2018), there is no onshore-offshore gradient, whereas in summer (August 2017) and to a lesser degree in late fall (November 2017), spatial differences in onshore (93.3 28 and 93.3 30) and offshore (93.3 35 and 93.3 40) environmental profiles are evident. These spatial differences are most pronounced in late summer (August 2017). Additionally, in August 2017 there is evidence of some unusual vertical structure in the oxygen profile around 200 m; both at station 93.3 28 and 93.3 30. Our first deployment (D200-LJ-1) was conducted in late August, so may have captured part of this feature. However, this cannot fully explain the higher variability we observed at 200 m, because our later deployment (D200-DM) was done in mid November, when there is no evidence of unusual vertical structure in the oxygen profile at 200 m for 93.3 28 or 93.3 30.